Secondary Organic Aerosols from OH Oxidation of Cyclic Volatile Methyl Siloxanes as an Important Si Source in the Atmosphere

Chong Han[1,2], Hongxing Yang[1], Kun Li[2,3], Patrick Lee[2], John Liggio[2], Amy Leithead[2], Shao-Meng Li[4]*

[1]School of Metallurgy, Northeastern University, Shenyang, 110819, China

[2]Air Quality Research Division, Environment and Climate Change Canada, Toronto, Ontario M3H 5T4, Canada

[3]Laboratory of Atmospheric Chemistry, Paul Scherrer Institute, Villigen 5232, Switzerland

[4]State Key Joint Laboratory of Environmental Simulation and Pollution Control, College of Environmental Sciences and Engineering, Peking University, Beijing, China 100871

Correspondence: Shao-Meng Li (shaomeng.li@pku.edu.cn)

Short summary: We presented yields and compositions of Si-containing SOA generated from the reaction of cVMS (D3-D6) with OH radicals. NO_x played negative roles on cVMS SOA formation, while ammonium sulfate seeds enhanced D3-D5 SOA yields at short photochemical ages under high-NO_x conditions. The aerosol mass spectra confirmed that the components of cVMS SOA significantly relied on OH exposure. A global cVMS-derived SOA source strength was estimated to understand SOA formation potentials of cVMS.

Abstract

Cyclic volatile methyl siloxanes (cVMS) are active ingredients in widely used consumer products, which can volatilize into the atmosphere, thus attracting much attention due to their potential environmental risks. While in the atmosphere the cVMS undergo oxidation yielding both gaseous and particulate products. The aerosol yields and compositions from the OH oxidation of four cVMS (D3-D6) were determined under low

and high-NO_x conditions in an oxidation flow reactor. The aerosol yields progressively increased from D3 to D6, consistent with the volatilities and molecule weights of these cVMS. NO_x can restrict the formation of SOA, leading to lower SOA yields under high-NO_x conditions than under low-NO_x conditions, with a yield decrease between 0.05-0.30 depending on the cVMS. Ammonium sulfate seeds exhibited minor impacts on SOA yields under low-NO_x conditions, but significantly increased the SOA yields in the oxidation of D3-D5 at short photochemical ages under high-NO_x conditions. The mass spectra of the SOA showed a dependence of its chemical compositions on OH exposure. At high exposures, equivalent to photochemical ages of > 4 days in the atmosphere, D4-D6 SOA mainly consisted of C_xH_y and $C_xH_yO_zSi_n$ under low-NO_x conditions, whereas they primarily contained N_mO_z, C_xH_y, $C_xH_yO_1$, $C_xH_yO_{>1}$ and $C_xH_yO_zSi_n$ under high-NO_x conditions. The potential contributions of cVMS to SOA formation in the atmosphere were evaluated using the reported cVMS annual production and the yield data obtained in the present study. A global cVMS-derived (D4-D6) SOA source strength is estimated to be 0.01 Tg yr^{-1}, distributed over major urban centers.

1 Introduction

Secondary organic aerosols (SOA), which contribute 50-85% to the mass of atmospheric organic aerosols (OA) (Glasius and Goldstein, 2016), are mainly formed via the partitioning of low volatility products from oxidation of volatile organic compounds (VOCs), semi- and intermediate volatile organic compounds(S/IVOCs) (Riipinen et al., 2012). SOA has attracted significant attention due to their important impacts on climate, ecosystems and human health (Berndt et al., 2016). Global budgets of SOA remain an unresolved issue despite extensive research, largely due to uncertainties associated with aerosol yields and the presence of unconsidered SOA precursors.

As one type of anthropogenic VOC and potential SOA precursors, cyclic volatile methyl siloxanes (cVMS)

45 are widely used in industrial applications and personal care products (Genualdi et al., 2011; Krogseth et al.,
46 2013a). cVMS have been classified as high-volume chemicals with an annual production of millions of tons
47 globally (Rücker and Kümmerer, 2015; Ahrens et al., 2014). Studies of cVMS in the environment have
48 focused on investigating health and environmental impacts particularly due to their potential persistence,
49 bioaccumulation and toxicity (Guo et al., 2019; Liu et al., 2018; Farasani and Darbre, 2017; Xu et al., 2019;
50 Kim et al., 2018; Coggon et al., 2018). As a result, the European Council has proposed a restriction on the
51 octamethylcyclotetrasiloxane (D4) and decamethylcyclopentasiloxane (D5) content in wash-off personal
52 care products to a limit of 0.1 mass% by 2020 (Eur-Lex, 2018). The legislative actions notwithstanding,
53 knowledge of environmental behavior of cVMS still needs to be further deepened as compared to their
54 applications and economic significance (Rücker and Kümmerer, 2015).
55 It has been estimated that approximately 90% of cVMS are emitted into the atmosphere due to their high
56 saturation vapor pressures (Allen et al., 1997). Gas-phase cVMS have been observed in both indoor and
57 outdoor air. Tang et al. (2015) reported that cVMS accounted for about one-third of total VOC mass
58 concentration in a classroom. Outdoor air concentrations of cVMS have also been measured at different sites
59 worldwide (Li et al., 2020; Wang et al., 2018; Rauert et al., 2018), increasing from rural to urban sites and
60 consistent with increasing population density (Rücker and Kümmerer, 2015). For example, at a rural site in
61 Sweden, the concentration of hexamethylcyclotrisiloxane (D3), D4, D5 and dodecamethylcyclohexasiloxane
62 (D6) were 0.94, 3.5, 13 and 1 ng/m^3, respectively (Kierkegaard and Mclachlan, 2013), while they were 18,
63 55, 172 and 14 ng/m^3 in urban areas of Toronto in Canada, respectively (Genualdi et al., 2011; Rauert et al.,
64 2018). cVMS have also been detected in the remote Arctic atmosphere, confirming their long-range transport
65 (Genualdi et al., 2011; Krogseth et al., 2013b). Atmospheric half-lives of cVMS are on the order of 30, 15,
66 10 and 6 days for D3-D6, respectively, which allow cVMS to exhibit a hemispherical distribution in the

atmosphere (Canada, 2008; Xiao et al., 2015). These lifetimes are driven mostly by reactions with the OH radicals (Xiao et al., 2015; Wang et al., 2013), which generate silanols and dimeric products that can be partitioned to condensed phases (Coggon et al., 2018; Sommerlade, 1993; Wu and Johnston, 2016). Different OH concentrations can partly explain the seasonal variation of cVMS lifetimes that was characterized by longer during winter than in summer (Rücker and Kümmerer, 2015). The loss of cVMS in the atmosphere is negligible through O_3 and NO_3 due to their small reaction rates (Atkinson, 1991). The global loss by the reaction with Cl atoms is less than 5% on account of low Cl concentrations, although it may be higher in some regions where cVMS emissions and Cl sources overlap in both space and time (Alton and Browne, 2020). It has been demonstrated that elemental Si is a frequent constituent of nanoparticles in rural and urban areas (Phares et al., 2003; Rhoads, 2003; Bein, 2005; Bzdek et al., 2014) and in remote regions (Li and Winchester, 1990; Li and Winchester, 1993). These Si-containing nanoparticles have previously been attributed to ore smelting processes, but recent studies have shown that Si-containing species are one of the main components in cVMS SOA, suggesting that the oxidation of cVMS may be an important source of Si in atmospheric aerosols (Wu and Johnston, 2016, 2017). In a modeling study, the oxidation products of cVMS (D4, D5 and D6) were considered to quantify the maximum potential for aerosol formation through reactions with the OH radicals (Janechek et al., 2017). Chandramouli and Kamens (2001) demonstrated the gas-particle partitioning of silanols from D5 oxidation by the OH radicals. Wu and Johnston (2016, 2017) analyzed the chemical composition of secondary aerosols from OH oxidation of D4 and D5, showing a large number of monomeric and dimeric products. Janechek et al. (2017, 2019) reported physical properties of SOA generated by OH oxidation of D5, including hygroscopicity, cloud seeding potential and volatility. Charan et al. (2022) measured SOA yields of D5 using chambers and flow tube reactors, emphasizing the importance of the relevant OH concentrations and exposures when extrapolating these laboratory results or

comparing with other studies. These studies mainly focused on D5 and occasionally D4 but rarely others. To better understand the SOA-forming potentials of typical cVMS in the atmosphere, accurate yields and molecular compositions of SOA from the oxidation of cVMS under various atmospheric conditions are needed.

In this work, the formation of SOA from the oxidation of four cVMS (D3-D6) by OH radicals was investigated in an oxidation flow reactor (OFR). Under various combinations of NO_x and ammonium sulfate seed concentrations, the yields and compositions of SOA formed from the oxidation were measured using a suite of instruments including a scanning mobility particle sizer (SMPS), a proton transfer reaction time of flight mass spectrometer (PTR-ToF-MS) and an aerosol mass spectrometer (AMS). Based on these SOA yields, the contribution of cVMS to SOA in the global atmosphere was estimated using reported cVMS concentrations. The results obtained here can largely improve our understanding of the contribution and composition of SOA from cVMS.

2 Experiments and methods

2.1 Photo-oxidation experiments

The reactions of cVMS with OH radicals were controlled at a constant temperature (21±1˚C) and relative humidity (35%±2%) in a custom-made oxidation flow reactor (the Environment and Climate Change Canada oxidation flow reactor, ECCC-OFR), which is shown in Fig. S1 of the Supplement and has been described in detail previously (Li et al., 2019a). Briefly, the ECCC-OFR is a fused quartz cylinder (length: 50.8 cm, inner diameter: 20.3 cm) equipped with a conical inlet and 7 outlets. Wall losses of particles and gases in the ECCC-OFR have been shown to be lower than in other OFRs (Huang et al., 2017; Lambe et al., 2011; Simonen et al., 2017; Li et al., 2019a). The length and full angle of cone inlet are 35.6 cm and 30°, respectively, designed to minimize the formation of jetting and recirculation in the OFR. The outlet at the

reactor center is a stainless-steel sampling port (inner diameter: 0.18 in) extending 12.7 cm long into the ECCC-OFR. This sampling inlet reduces the impact of potential turbulent eddies caused by the back end of the reactor. The remaining 6 outlets around the perimeter are designed to allow side flows to pass through the OFR as a sheath flow, indirectly reducing wall losses of gases and particles inside the OFR upon sampling. Ozone-free mercury UV lamps for generating OH radicals are housed in small quartz tubes around and in parallel to the quartz reaction cylinder, and a large flow of air through each of these smaller quartz tubes is used to remove the heat produced by the lamps. The relative humidity was adjusted by controlling the ratio of dry air to wet air into the reactor, and was measured using a humidity sensor (Vaisala) at one of the sheath flow outlets (side flows) of the reactor. The volume of the entire ECCC-OFR is about 16 L and the total flow rate is 8 L min^{-1}, leading to a residence time of 2 min in the OFR.

OH radicals were produced through the reaction of water vapor with $O(^1D)$ formed from O_3 photolysis at 254 nm. The OH concentration in the ECCC-OFR was regulated by controlling the input voltage and the number of UV lamps. Methanol vapor, introduced into the ECCC-OFR through a bubbler containing methanol solution, was used to determine the OH exposure (i.e., photochemical age, from the multiplication of OH concentration and reaction time) by tracking its decay in the reactor from the reaction with the OH. The decay, or fractional loss, of gas-phase methanol, $[MeOH]/[MeOH]_0$ was measured with the PTR-ToF-MS, and was used to calculate the OH concentration via Equation 1,

$$[OH]=-\frac{1}{k_{MeOH}}\ln\frac{[MeOH]}{[MeOH]_0} \quad (1)$$

where k_{MeOH} is the second-order rate constant of methanol reaction with OH at 298 K (9.4×10^{-13} cm^3 $molecule^{-1}$ s^{-1}). The OH exposure measurement was offline, because methanol can affect the OH reactivity with cVMS. Under low and high-NO_x conditions described below, the OH exposure varied in the range of 5.5×10^{10}-1.8×10^{12} and 8.2×10^{10}-1.1×10^{12} molecules cm^{-3} s, respectively. They correspond to 0.4-14.2

and 0.6-8.5 equivalent days (photochemical age), respectively, assuming that an average OH concentration in air is 1.5×10^6 molecules cm^{-3} (Mao et al., 2009).

Pure D3-D6 cVMS compounds (solid D3 and liquid D4, D5 and D6) were placed in a glass U-type tube and maintained at room temperature. Vapors from these compounds (Table S1 of the Supplement) were separately introduced into the ECCC-OFR by a small flow of zero air (1-18 mL min^{-1}) passing over the headspace of the U-tube containing the pure compounds. The concentrations of D3-D6 in the ECCC-OFR ranged from 20 to 43 ppb (Table S2), depending on their volatilities. Table S2 summarizes the concentrations of cVMS at the reactor inlet and outlet, when the OH exposure was 1.85×10^{12} and 1.10×10^{12} molecules cm^{-3} s in low and high-NO_x experiments, respectively, indicating the reaction depth of cVMS. To study the influence of existing particles on the SOA formation, ammonium sulfate (AS) seed particles were produced using an atomizer, dried by a diffusion dryer and neutralized by a neutralizer and injected into the reactor without size selection. The mass concentration of AS seed particles was approximately 30 μg m^{-3} for all experiments.

N_2O was used as a source of NO to achieve high-NO_x conditions (Lambe et al., 2017). NO_x conditions were defined by the fate of peroxy radicals (RO_2), which was described by the reaction rate ratio (R_{NO}) of RO_2 + NO and RO_2 + HO_2 (Peng et al., 2018). The R_{NO} ratio increases with increasing OH exposures at a constant concentration of N_2O (Li et al., 2019b). To achieve a constant branching ratio during the high-NO_x experiments, the initial N_2O concentration in the OFR was varied (1.6%-8.0%) to maintain an R_{NO} value of 20 (Li et al., 2019b), as calculated using a model (OFR Exposures Estimator v3.1) (Peng et al., 2018). A ratio of R_{NO}=20 indicates that 95% of RO_2 reacts with NO, ensuring the dominance of RO_2 + NO, which represents conditions that are relevant for urban atmosphere (Peng et al., 2019). The role of RO_2 + RO_2 here should be minor or negligible due to the low concentration of SOA precursors (cVMS, 18-46 ppb) (Lambe

et al., 2017; Peng et al., 2019; Li et al., 2019b). Peng et al. (2019) have reported that in the experiments utilizing the injection of N_2O to achieve high-NO_x conditions, the relative importance of RO_2 + OH was generally negatively correlated with N_2O due to the suppressing effect of NO_x on OH radicals and the increasing role of RO_2 + NO. Under low-NO_x conditions, N_2O was not introduced into the OFR, where the reaction ratio of RO_2 with HO_2 was estimated to be larger than 99% according to the model mentioned above (Peng et al., 2018), representing atmospheric scenarios with few NO_x sources.

2.2 Characterization and analysis

The concentrations of cVMS in the OFR were measured online with PTR-ToF-MS (Ionicon Analytik GmbH) (Liggio et al., 2016). The number and mass size distribution of aerosols was monitored using a scanning mobility particle sizer (SMPS, TSI). The mass spectra and elemental composition of aerosols was determined with a high-resolution time-of-flight aerosol mass spectrometer (HR-ToF-AMS, Aerodyne) and analyzed with the AMS analysis software Squirrel (version 1.62G) and Pika (version 1.22G).

SOA mass yields (Y) were calculated via Equation 2,

$$Y = \frac{\Delta C_{\mathrm{SOA}}}{\Delta C_{\mathrm{cVMS}}} \quad (2)$$

where ΔC_{SOA} and ΔC_{cVMS} are the mass concentrations of SOA formed and cVMS lost, respectively. The mass concentration of SOA was determined by multiplying the effective aerosol density by the integrated SOA volume concentration from the SMPS, subtracting the AS seed volume for experiments with AS seeds. The effective aerosol density (ρ) was calculated for unseeded experiments through the following Equation 3 (Lambe et al., 2015),

$$\rho = \frac{D_{va}}{D_m} \quad (3)$$

where D_{va} is the vacuum aerodynamic diameter obtained from the HR-ToF-AMS, and D_m is the electric mobility diameter measured by the SMPS. The ρ varied in the range of 1.6-1.8 depending on the cVMS. The

same ρ value was also used in the seeded experiments. It should be pointed out that the background values in Table S3 have been subtracted when calculating the cVMS SOA yields. The average data of SMPS and AMS in the last ~10 minutes for each OH exposure was used to calculate the SOA yields (inset of Fig S2), which can reduce the deviation caused by unstable SOA loadings at high OH exposures.

3 Results and discussion

3.1 SOA yields

Taking the D5 SOA under unseeded conditions as an example, the number and mass size distributions of aerosols were shown in Fig. S3 at three photochemical ages (PA), i.e., time-integrated OH exposure. It can be seen that small particles dominated the total particle number counts, while large ones dominated the mass. The mass mode diameter of SOA for mass size distributions increased with PA under low and high-NO_x conditions. The mass concentrations and time series of SOA obtained from SMPS and AMS were shown in Table S4 and Fig. S2, respectively, which reflected a step-by-step pattern with increasing OH exposures. Unstable SOA loadings at high OH exposures may be attributed to the fragmentation reactions, leading to the difficulty in the deposition of products on SOA.

Figure 1 shows the SOA yields from the photooxidation of the D3-D6 cVMS under low and high-NO_x conditions as a function of PA, with and without AS seed particles. SOA yields have been widely used to estimate the potential of precursors to produce aerosol mass (Mcfiggans et al., 2019; Li et al., 2019a; Bruns et al., 2015; Lambe et al., 2015). As shown in Fig. 1, the cVMS SOA yields exhibited an overall increasing trend with PA, expressed in equivalent photochemical days, which agreed with the trend of D5 SOA yields reported by Janechek et al. (2019). Under low-NO_x conditions (Fig. 1a), SOA yields exhibited a slow growth, reaching a plateau after 10 equivalent days. This may be due to increased gas-phase fragmentation of cVMS to generate some higher volatility products, leading to a small increasing amplitude of partition ratio of

199 species into SOA at longer photochemical ages.

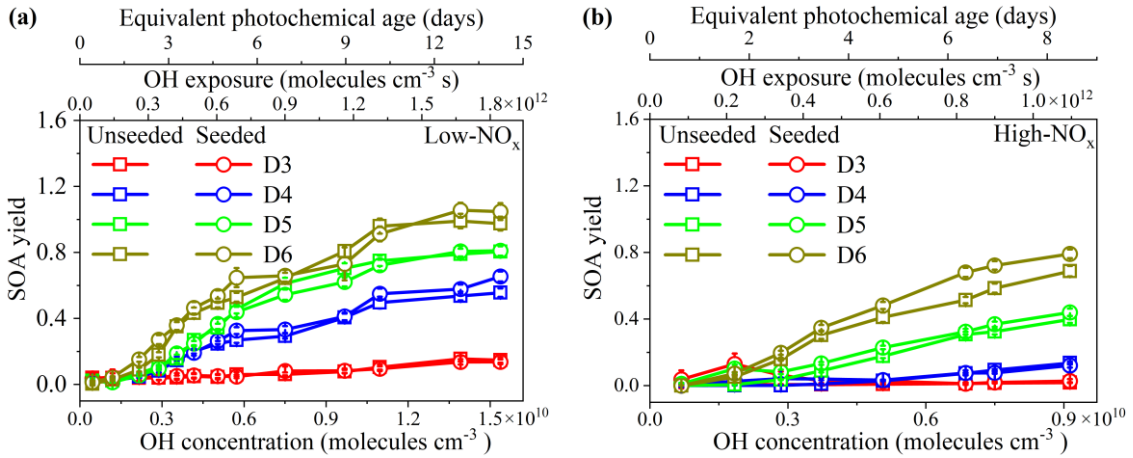

200

201 Figure 1. SOA yields from unseeded and seeded (30 μg m^{-3}) photooxidation of cVMS by OH radicals. (a)

202 low-NO_x experiments; (b) high-NO_x experiments.

203

204 For the unseeded and low-NO_x experiments in Fig. 1a, SOA yields of four cVMS exhibited significant

205 differences in values over the same number of equivalent days. The SOA yields successively increased from

206 D3 to D6, consistent with the volatilities and molecular masses of the cVMS as well as their reaction rate

207 constants with the OH radical (Alton and Browne, 2020; Kim and Xu, 2017; Safron et al., 2015). The

208 maximum SOA yields of D3-D6 were (0.16±0.02), (0.56±0.03), (0.80±0.03) and (0.99±0.04), respectively,

209 occurring after a PA of 12 equivalent days. It has been reported that D5 SOA yields varied in the range of 0-

210 1.1 (Janechek et al., 2019; Wu and Johnston, 2017; Charan et al., 2022). Under a low OH exposure (~10^{10}-

211 10^{11} molecules cm^{-3} s), the D5 SOA yield (0.01-0.11) obtained here was similar to that (chamber, 0-0.057;

212 flow tube, 0.018-0.06) measured by Charan et al. (2022). However, under a high OH exposure of ~10^{11}-10^{12}

213 molecules cm^{-3} s, the D5 SOA yield of 0.46-0.70 was higher than 0.22 and 0.14-0.35 (flow tube) reported

214 by Janechek et al. (2019) and Charan et al. (2022), respectively, which may be attributed to differences in

215 experimental conditions, such as differences in reactors, wall losses, SOA measurement methods,

216 determination of OH concentrations, and initial D5 concentrations (Table S5) (Janechek et al., 2019; Charan

et al., 2022). Although the amount of cVMS lost was variable, cVMS SOA yields positively depended on SOA mass concentrations (Fig. S4), and this trend was observed in previous D5 SOA experiments with OH oxidation (Wu and Johnston, 2017).

As shown in Fig. 1b, the order of SOA yields from the four cVMS under high-NO_x conditions was the same as that under low-NO_x conditions. However, the SOA yields under high-NO_x conditions were generally smaller than the corresponding yields at similar OH exposures under low-NO_x conditions, with a decrease of 0.05-0.30 depending on the cVMS. Such a reduction suggests that NO_x can restrict the formation of cVMS SOA. NO_x has been shown to reduce SOA yields for some anthropogenic alkanes (Li et al., 2019b), aromatics (Ng et al., 2007a; Chan et al., 2009; Zhou et al., 2019), monoterpenes (Zhao et al., 2018) and other terpenes (Ng et al., 2007b), attributable to the formation of higher volatility products (e.g., organic nitrates) generated by RO_2 + NO compared to RO_2 + HO_2 (Presto et al., 2005; Li et al., 2019b), which is also likely the case here. The higher volatility products favor partitioning in the gas phase, thus reducing the potential for forming SOA (Zhou et al., 2019). Moreover, high NO_x levels can suppress the formation of products for nucleation, thereby reducing aerosol surface as a condensational sink and increasing the wall loss of condensable species in an OFR under high-NO_x conditions (Zhao et al., 2018; Sarrafzadeh et al., 2016; Wildt et al., 2014). Figure S5 indicates that the difference between SOA yields with and without NO_x decreased with increasing silicon atoms within individual cVMS, indicating a less restricting effect of NO_x on the SOA formation for larger cVMS. This means that high NO_x levels play a lessor role in the SOA yields of lower volatility precursors.

SOA yields in the AS-seeded experiments under low and high-NO_x conditions are also shown in Figs. 1 and S5, indicating minimal impacts of the AS seed particles on SOA yields. A yield enhancement ratio ($R_E = Y_{seeded}/Y_{unseeded}$, Fig. S6) was used to show the seed impacts more clearly. Under low-NO_x conditions,

239 the R_E values for all cVMS were close to 1.0 (Fig. S6a), suggesting a negligible impact of AS seed particles
240 on SOA yields; however, under high-NO_x conditions, R_E was much larger (17.81, 13.18 and 15.51 for D3-
241 D5, respectively) at short PA but gradually decreased to 1.0 with increasing PA for D3-D5, while it was
242 always close to 1.0 for D6 regardless of PA (Fig. S6b). R_E values greater than 1.0 suggest that AS seed
243 particles played an enhancement role in the cVMS SOA formation, as similarly reported in SOA formation
244 from hydrocarbons (Sarrafzadeh et al., 2016; Lamkaddam et al., 2017; Li et al., 2019b). Under low-NO_x
245 conditions, the general lack of impact on cVMS SOA yields by the AS seed particles suggests that
246 condensation was not the main process driving SOA formation in cVMS oxidation. For the few cases of high
247 NO_x level at low PA, where R_E was >1 for D3-D5, it is possible that their early generations of oxidation
248 products were more volatile than successive generations of products and hence more prone to condensation
249 enhanced by AS seeds. As PA increased, further reactions of these early generation oxidation products with
250 OH radicals resulted in further generation products that were likely less volatile, thereby weakening the
251 enhancing role of AS seeds at high OH exposure. Such effect was less pronounced for D6, likely because its
252 oxidation products at different PA had similar volatilities. Figure S6b shows that the effect of AS seed
253 particles on SOA yields negatively correlated with the number of silicon atoms in the cVMS. Lower volatility
254 precursors (D5 and D6) may form lower volatile products, resulting in SOA yields less sensitive to the pre-
255 existing seeds.

256 **3.2 Aerosol compositions**

257 **3.2.1 Compositions of SOA under low-NO_x conditions.**

258 Figures 2 and S7 show the normalized HR-ToF-AMS mass spectra of cVMS SOA from unseeded
259 experiments under low-NO_x conditions at OH exposures of 9.0×10^{11} molecules cm^{-3} s (i.e., OH
260 concentration of 7.5×10^9 molecules cm^{-3}). The mass spectral signals can be identified as fragments with a

formula of $C_xH_yO_zSi_n$. For D3 SOA, the most prominent peaks were at m/z 44 and 29, dominated by CO_2^+ and CHO^+, which were tracers for organic acids (Ng et al., 2010), alcohols and aldehydes (Lee et al., 2012), respectively. They may result from the oxidation of the methyl groups in D3 by OH radicals. For the mass spectra of D4-D6 SOA, the two highest peaks at m/z 14 and 15 were CH_2^+ and CH_3^+, respectively. In addition, there were several dominant $C_xH_yO_zSi_n$ peaks, which were fragments of silicon-containing products. For the $C_xH_yO_zSi_n$ group in D4 SOA, there were four typical peaks at m/z 255, 257, 271 and 273, with formulae of $C_4H_{11}O_7Si_3^+$, $C_3H_9O_8Si_3^+$, $C_3H_7O_9Si_3^+$ and $C_3H_9O_9Si_3^+$, respectively. The $C_xH_yO_zSi_n$ fragment group containing Si of D5 SOA had three dominant peaks at m/z 327, 329 and 331, corresponding to $C_{12}H_{11}O_2Si_5^+$, $C_9H_9O_8Si_3^+$ and $C_5H_{15}O_9Si_4^+$, respectively. For the $C_xH_yO_zSi_n$ group containing Si in D6 SOA, there were five main peaks at m/z 73 (C_3H_9Si), 387 ($C_8H_{23}O_8Si_5^+$), 389 ($C_8H_9O_9Si_5^+$), 401 ($C_9H_{21}O_{10}Si_4^+$) and 403 ($C_7H_{15}O_{12}Si_4^+$).

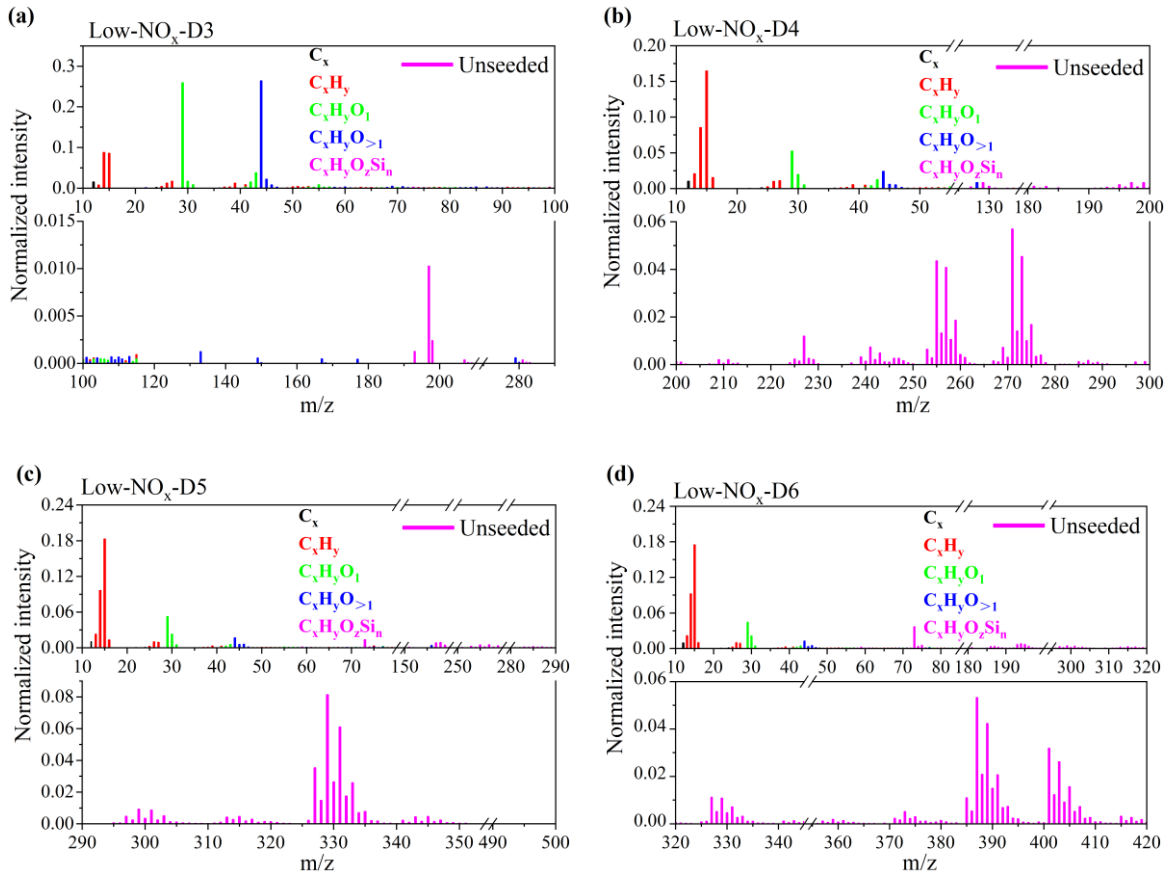

Figure 2. HR-ToF-AMS mass spectra of cVMS SOA at OH exposure of 9.0×10^{11} molecules cm^{-3} s (i.e., OH concentration of 7.5×10^{9} molecules cm^{-3}) under low-NO_x conditions in unseeded experiments. a-d represent the mass spectra of D3-D6 SOA, respectively.

Figure 3 shows the evolution of different groups of ions in the HR-ToF-AMS spectra of the cVMS SOA as a function of PA in equivalent days. For D3-D6 under unseeded conditions, $C_xH_yO_1$ and $C_xH_yO_{>1}$ ions significantly decreased within 0-4 equivalent days of PA, but remained essentially unchanged when PA increased to 7-15 equivalent days. The C_xH_y ion increased to its peak value at about 9 equivalent days of PA for D3 and 2-3 equivalent days of PA for D4-D6, and then gradually decreased with further PA increases. The $C_xH_yO_zSi_n$ group of ions maintained an increasing trend until 9-10 days of PA, thereafter it decreased slightly for D4-D6 SOA.

285 The weighted values of the Si/C (n/x) and Si/O (n/z) atomic ratios for the $C_xH_yO_zSi_n$ groups in D5 and D6
286 SOA at different PA are plotted in Fig. S8 (Detailed calculations in Text S1 of the Supplement), which can
287 be used to indicate the changes in the Si element of SOA. The Si/C ratio increased slightly with increasing
288 PA, whereas the Si/O ratio had an overall decrease trend. While it is difficult to separate the effect of
289 fragmentation due to the AMS ionization process, the relative changes of group intensities and the evolution
290 of Si/C and Si/O in $C_xH_yO_zSi_n$ over different PA may be attributed to the evolution of cVMS when oxidized
291 by the OH radicals. The initial step of OH radical oxidation is H abstraction from the methyl groups on the
292 -Si-O- ring of the cVMS to form Si-containing radicals, which may generate OH and CH_2OH substitution
293 products, such as silanol and silyl methanol (Wu and Johnston, 2016; Alton and Browne, 2020). Such Si-
294 containing products may partition into SOA and result in an appearance of $C_xH_yO_zSi_n$ ions in the AMS mass
295 spectra. Notably, it was reported that one of oxidation products of D5, 1-
296 hydroxynonamethylcyclopentasiloxane (D_4TOH), has been detected in ambient particulate matter (Milani et
297 al., 2021). At low PA, some oxygen-containing functional groups (-CH_2OH/-COOH/-OH), which were
298 formed by the reaction of methyl groups in cVMS with OH, resulted in a decrease of Si/O ratio. The Si-O
299 bond breaking may mainly happen at high OH exposures, and it may occur after the cleavage of Si-C bonds
300 (Rücker and Kümmerer, 2015). According to the previous study of Wu and Johnston (2017), some ring-
301 opened products were generated from the reaction of D5 with OH radicals, necessarily requiring the cleavage
302 of Si-O bonds. The Si-O bond cleavage from the OH radical attack may reduce the number of Si atoms,
303 leading to a continuous decrease of Si/O at high PA. The continued breaking of Si-O bonds would lead to
304 fragmentation and more volatile products, which caused lower SOA yield and $C_xH_yO_zSi_n$ fraction at longer
305 PA (Figs. 1 and 3). The field measurements observed that Si acts as a frequent component of atmospheric
306 nanoparticles (Bzdek et al., 2014). This work further determines that cVMS SOA could become an important

contributor to Si in aerosols.

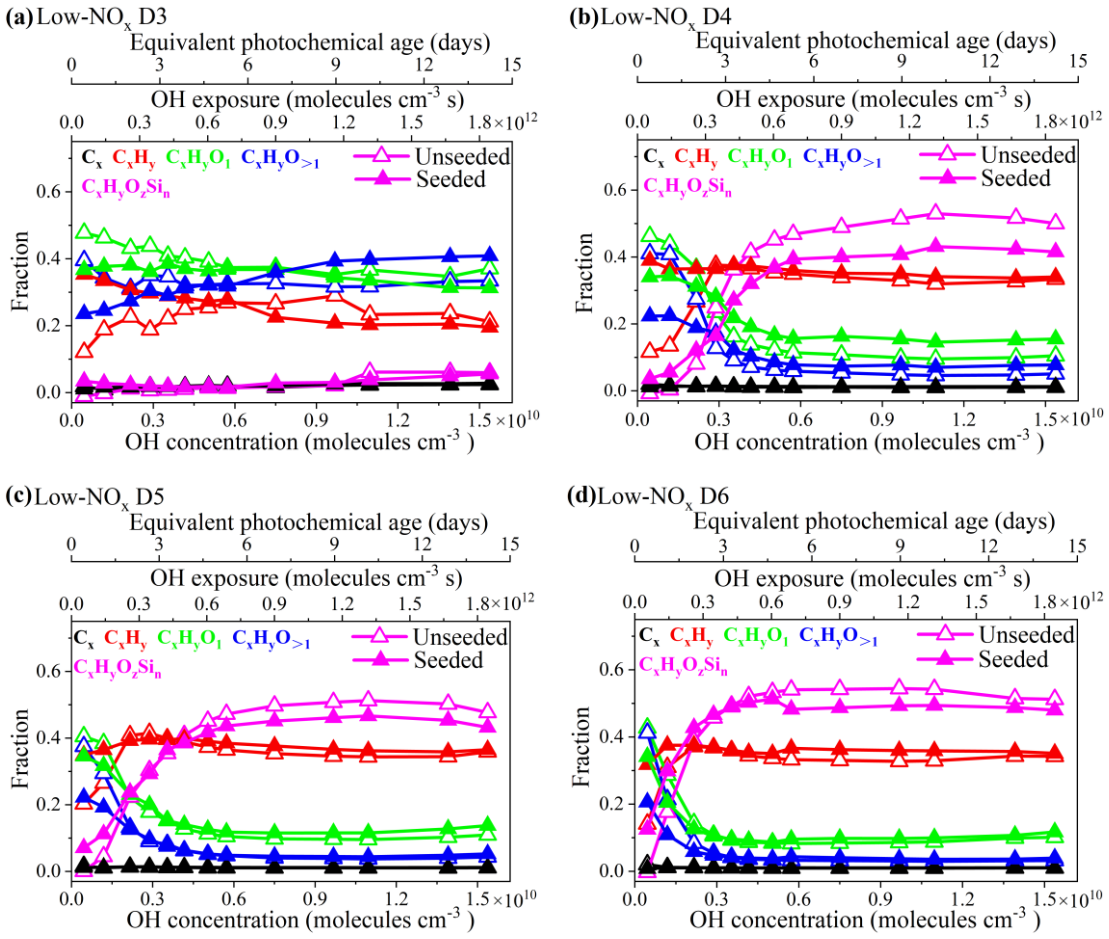

Figure 3. Fraction of C_x, C_xH_y, $C_xH_yO_1$, $C_xH_yO_{>1}$ and $C_xH_yO_zSi_n$ ion groups for SOA derived from the oxidation of cVMS (a-d) by OH radicals at different photochemical ages under low-NO_x conditions. Empty and solid triangles represent experimental data under unseeded and seeded conditions, respectively.

As shown in Fig. 3, the presence of seeds led to some changes in the evolution trends of ion groups in the AMS spectra. For instance, the initial fraction of C_xH_y in seeded experiments was larger than that in unseeded experiments, which may be related to the volatility of species containing C_xH_y that may be more easily deposited in the presence of seeds, whereas $C_xH_yO_1$ and $C_xH_yO_{>1}$ exhibited opposite changes. The presence of seeds led to larger initial and smaller steady-state $C_xH_yO_zSi_n$ fractions than those in unseeded experiments. Regardless of the presence of seeds, C_xH_y, $C_xH_yO_1$ and $C_xH_yO_{>1}$ mainly contributed to the composition of

all cVMS SOA at initial OH radicals oxidation, but D4-D6 SOA primarily consisted of C_xH_y and $C_xH_yO_zSi_n$ after 4 equivalent days.

3.2.2 Compositions of SOA under high-NO_x conditions.

Figure S9 shows the HR-ToF-AMS mass spectra of cVMS SOA from unseeded experiments under high-NO_x conditions at OH exposures of 9.0×10^{11} molecules cm^{-3} s (~6.9 d). Compared to that under low-NO_x conditions (Figs. 2 and S7), there was one additional N-containing group (N_mO_z) in the SOA mass spectra under high-NO_x conditions, which accounted for 16%-31%. For the mass spectra of D3-D6 SOA originating from unseeded experiments under high-NO_x conditions in Fig. S9, the dominating peaks of the N_mO_z family were m/z 30 (NO^+) and m/z 46 (NO_2^+). The common main peaks were located at m/z 30 (NO^+) for cVMS SOA, m/z 44 (CO_2^+) for D3-D4 SOA, and m/z 46 (NO_2^+) for D4-D6 SOA. In addition, there were other primary peaks at m/z 29 (CHO^+) for D4 SOA, while m/z 15 (CH_3^+) and m/z 28 (CO^+) for D5-D6 SOA. The m/z 28 (CO^+), similar to m/z 44 (CO_2^+), is considered as a tracer for organic acids (Ng et al., 2010). In the mass spectra for D3-D6 SOA under high-NO_x conditions, the presence of NO^+ (m/z 30) and NO_2^+ (m/z 46) illustrated the formation of organic or inorganic nitrates in SOA (Ng et al., 2007b; Zhao et al., 2018).

For the $C_xH_yO_zSi_n$ group in the D4 SOA mass spectrum under high-NO_x conditions, the dominating peaks and their formulas were the same as those under low-NO_x conditions. For the $C_xH_yO_zSi_n$ group in D5 SOA, in addition to two typical peaks at m/z 327 and 329 in the low-NO_x experiments, there was another prominent peak at m/z 328, with a formula $C_8H_{12}O_5Si_5$. The $C_xH_yO_zSi_n$ group in D6 SOA had three typical peaks at m/z 73 (C_3H_9Si), m/z 387 ($C_8H_{23}O_8Si_5^+$) and m/z 401 ($C_9H_{21}O_{10}Si_4^+$). For the $C_xH_yO_zSi_n$ groups in cVMS SOA, there was little difference in the x, y, z and n value assignment of $C_xH_yO_zSi_n$ peaks in SOA generated under low-NO_x and high-NO_x conditions, suggesting the formation of similar Si-containing oxidation products.

For cVMS SOA under high-NO_x conditions, the evolution of family groups as a function of OH exposure

342 was summarized in Fig. S10. The dominant composition at the initial stage was $C_xH_yO_{>1}$ groups for D3-D6
343 SOA. At equivalent days larger than 4, D3 SOA primarily consisted of $C_xH_yO_{>1}$, N_mO_z and $C_xH_yO_1$ groups,
344 while D4-D6 SOA was mainly composed of $C_xH_yO_zSi_n$, N_mO_z, $C_xH_yO_1$, C_xH_y and $C_xH_yO_{>1}$ groups. Figure
345 S10 also shows influences of seeds on the evolution of family groups under high-NO_x conditions. It was
346 observed that all groups in D3-D6 SOA displayed similar change trends regardless of the existence of seeds.
347 As shown in Fig. S11, the trend of the Si/O ratio in the $C_xH_yO_zSi_n$ groups at different photochemical ages
348 under high-NO_x conditions was similar to that in low-NO_x experiments. However, the Si/C ratios remained
349 almost unchanged, and were close to the initial value (0.5) in cVMS. This may be attributed to the possible
350 suppression of cleavage of methyl groups from the -Si-O- ring of the cVMS under high-NO_x conditions.

351 **4 Conclusions and implications**

352 The yields and compositions of SOA generated from the photooxidation of four cVMS (D3-D6) with OH
353 radicals were investigated using an oxidation flow reactor. cVMS SOA yields exhibited an overall increasing
354 trend with PA, and their values gradually increased with cVMS from D3 to D6. SOA formations depended
355 on NO_x, as shown by smaller SOA yields under high-NO_x conditions. Ammonium sulfate seeds significantly
356 enhanced SOA yields of D3-D5 at short PA under high-NO_x conditions. The SOA mass spectra showed that
357 Si-containing species were one of main chemical compositions at PA > 4 days.

358 To evaluate the potential contributions of cVMS to SOA formation in the atmosphere, global SOA
359 concentrations produced from cVMS were estimated according to the cVMS SOA yields measured in this
360 work and using the cVMS concentrations reported from multiple studies, which were listed in Table S6.
361 Figure 4 shows the global concentration distribution of SOA from four cVMS (D3-D6) at 36 sites worldwide
362 estimated by the Equation 4,

363 $$C_{\text{cVMS-SOA}} = C_{\text{cVMS}} \times \frac{\Delta C_{\text{cVMS}}}{C_{\text{in-cVMS}}} \times Y \quad (4)$$

where C_{cVMS} and $C_{cVMS\text{-}SOA}$ are the mass concentration of cVMS reported from literatures and cVMS SOA estimated in global sites, respectively; $C_{in\text{-}cVMS}$ and ΔC_{cVMS} are the mass concentration of initial and lost cVMS at the selected equivalent days during the experiments of this work, respectively (Table S7); Y is the cVMS SOA mass yields selected here. The estimations from the Equation 4 were based on assumptions that the lost cVMS ratio is not affected by the cVMS concentration and the background $C_{cVMS\text{-}SOA}$ is zero. The dilution of cVMS would occur during the transportation in the atmosphere, leading to an uncertainty of cVMS concentrations (C_{cVMS}) in the Equation 4. To simplify the estimation process, the effect of dilution on C_{cVMS} would not be taken into account, and the reported C_{cVMS} values were directly used. It was noted that the time-integrated consumption over the lifetime of a precursor compound in the atmosphere should be suitable for evaluating the SOA formation. Accordingly, when considering atmospheric half-lives (6-30 days) of cVMS, the $\Delta C_{cVMS}/C_{in\text{-}cVMS}$ values in low-NO_x and unseeded experiments at 14.2 equivalent days (Table S7) are used to calculate cVMS SOA at background and polar sites. Due to a short residence time of airmass over urban areas, the $\Delta C_{cVMS}/C_{in\text{-}cVMS}$ values in high-NO_x and seeded experiments at 0.63 equivalent days (Table S7) are employed to estimate cVMS SOA at urban sites.

It should be noted that OH concentrations and exposures have different effects on the reaction systems, leading to different SOA yields. Under an ideal condition, a low OH concentration for a long exposure time and a high OH concentration for a short exposure time can achieve the same degree of degradation of the precursor compound. However, this is not applicable for the formation of SOA. Charan et al. (2022) have claimed that D5 SOA yields are dependent on the OH concentrations rather than OH exposures. When extrapolating the laboratory data to the real atmosphere, it is necessary to consider atmospherically relevant OH concentrations and exposures. Charan et al. (2022) also stated that the D5 SOA yield varied in a small range (0-6%) at the OH concentration $\leq 5 \times 10^8$ molecules cm^{-3}. It was assumed that the SOA yields at

environmentally relevant OH concentrations (~10^6 molecules cm^{-3}) were similar to those at the lowest OH concentrations (~10^8 molecules cm^{-3}) used here. Thus, the high-NO_x SOA yields (D3: 0.038; D4: 0.001; D5: 0.011; D6: 0.000) under the seeded conditions at the OH concentration of 6.83×10^8 molecules cm^{-3} (0.63 equivalent days) were employed in the calculation of cVMS SOA concentrations at urban sites, while the low-NO_x SOA yields (D3: 0.041; D4: 0.013; D5: 0.023; D6: 0.004) under the unseeded conditions at the OH concentration of 4.57×10^8 molecules cm^{-3} (0.42 equivalent days) were used to estimate cVMS SOA at background and polar sites. Although there may be some uncertainties in extrapolating our results to the real atmosphere, these extrapolations may still provide an estimation for understanding the SOA potential of cVMS.

Table S6 summarizes the details regarding sites and concentrations of cVMS SOA. The derived concentrations of cVMS SOA vary significantly among urban, background and polar sites. The total cVMS SOA concentrations in urban areas are the highest, up to 33.52 ng/m^3, which was comparable with the maximum cVMS SOA formation (21 ng/m^3) reported by Pennington et al. (2021) using the CMAQ model for Los Angeles. They are 0.57-8.86 and 0.37-1.97 ng/m^3 for background and Arctic sites, respectively. cVMS SOA concentrations in urban regions of Asia (sites 29-36) and Europe (sites 26-28) are generally larger than that of North America (sites 20-25). In China, the total cVMS SOA concentrations in urban sites range from 0.11 to 33.52 ng/m^3. The main precursors of cVMS SOA are different among Chinese cities. For three cities along the southeast coast of China (Guangzhou, Macau and Foshan), the dominant precursors of cVMS SOA are D3 and D4, which are related to industrial emissions of these two siloxanes in this region (Wang et al., 2001). For Dalian in China, D5 mainly contributes to cVMS SOA, and this can be attributed to the industrial production and the use of personal care products in Dalian (Li et al., 2020). In the other Chinese urban areas with reported cVMS concentrations (Lhasa, Golmud, Kunming and Yantai), the total cVMS

SOA concentrations are considerably smaller than those in the urban areas above, with D5 acting as the main precursor, which may be ascribed to the relatively low population densities in these cities (Wang et al., 2018).

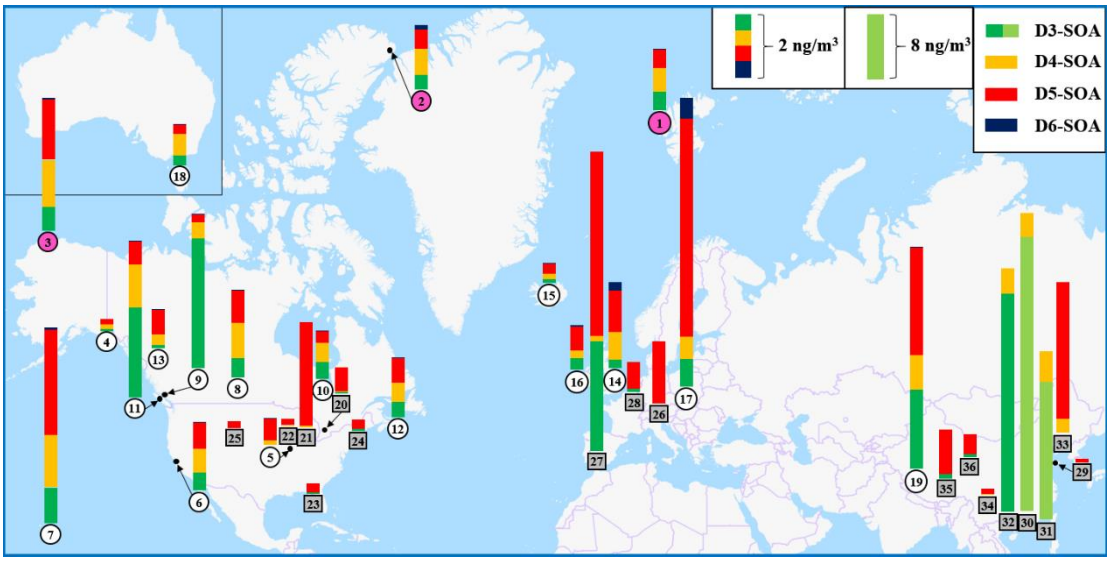

Figure 4. Global concentrations of cVMS SOA (ng/m^3) on the basis of the cVMS concentrations reported from multiple studies and the cVMS SOA yields measured in this work. The numbers of polar, background and urban sites are enclosed in pink, white circles and gray boxes, respectively. The details about cVMS and SOA concentrations at different sites were summarized in Table S6 of the Supplement.

At urban sites in Europe and North America, cVMS SOA concentrations are reported in the range of 0.91-9.16 ng/m^3 and 0.19-3.23 ng/m^3, respectively. Among these cVMS, D5 is the main contributor to cVMS SOA at these locations, averaging 89.1% of total cVMS SOA. For instance, D5 SOA is calculated to be 5.63 ng/m^3 in Catalan, Spain, 3.19 ng/m^3 in Chicago, USA, 1.89 ng/m^3 in Zurich, Switzerland and 0.81 ng/m^3 in Paris, France, where there are high levels of economic activities and high population densities. These results suggest that personal care products as a main source of D5 may be the most important anthropogenic origins of Si-containing SOA in Europe and North America. The D5 SOA concentration (0.11-5.63 ng/m^3) estimated here is larger than that (0.016-0.206 ng/m^3) reported by Milani et al. (2021), who obtained their data using

semi-quantified concentrations of D_4TOH (first-generation D5 SOA product) extracted from $PM_{2.5}$ samples in Atlanta and Houston. The difference may be mainly attributed to the missing analysis of multi-generation SOA products or dimers (Wu and Johnston, 2016, 2017).

At background and Arctic sites, cVMS SOA are primarily derived from D3, D4 and D5. The background sites are located in mountains, rural areas, forested areas, lakes and at high altitudes. The three highest cVMS SOA concentrations at background sites are located at Kosetice in the Czech Republic (8.86 ng/m^3), Tibetan Plateau in China (6.78 ng/m^3) and Hilo of Hawaii in the USA (5.97 ng/m^3), where the contribution percentages of SOA from D3-D5 are 92.8%, 99.9% and 99.0%, respectively. The cVMS SOA concentrations at the Alert site in Nunavut, Canada is the highest (1.97 ng/m^3) among the three locations in the Arctic, 92.4% of which is accounted for by D3-D5 SOA. The dominance of D3-D5 SOA in both background and the Arctic regions highlights their persistence in the atmosphere and the potential for long-range atmospheric transport.

The global annual production of D4, D5 and D6 is about 1, 0.1 and 0.01 Tg·yr^{-1}, respectively, and 90% of these cVMS is eventually released into the atmosphere (Li et al., 2020; Genualdi et al., 2011; Wang et al., 2013; Sakurai et al., 2019). Based on the results shown in Fig. 4, the annual production of cVMS (D4-D6) SOA was estimated to be 0.01 Tg·yr^{-1}, which was about 0.34% of SOA (2.9 Tg·yr^{-1}) produced from mobile source emissions in the USA and 33%-50% of SOA generated by Athabasca oil sands (0.02-0.03 Tg·yr^{-1}, one of the largest sources of anthropogenic secondary organic aerosols in North America) (Tkacik et al., 2014; Liggio et al., 2016). Moreover, it was 0.05% and 0.14% of isoprene-SOA (20 Tg·yr^{-1}) and monoterpenes-SOA (7 Tg·yr^{-1}) (typical biogenic SOA), respectively, indicating the potential importance of cVMS SOA (Jokinen et al., 2015). While these cVMS SOA sources may seem small, they can make substantially higher contributions to ambient air SOAs in population centers where cVMS compounds are primarily used.

Author contributions

CH designed and conducted all experiments; CH and HY analyzed the data and prepared the paper with contributions from KL, PL, JL, AL and SML. SML supervised the project.

Competing interests

The authors declare that they have no conflict of interest.

Acknowledgements

This project was supported by Environment and Climate Change Canada's Climate and Clean Air Program (CCAP); the National Natural Science Foundation of China (42077198); the LiaoNing Revitalization Talents Program (XLYC1907185); the Fundamental Research Funds for the Central Universities (N2025011).

References

Ahrens, L., Harner, T., and Shoeib, M.: Temporal Variations of Cyclic and Linear Volatile Methylsiloxanes in the Atmosphere Using Passive Samplers and High-Volume Air Samplers, Environ. Sci. Technol., 48, 9374-9381, https://doi.org/10.1021/es502081j, 2014.

Allen, R., Kochs, P., and Chandra, G.: Industrial Organosilicon Materials, Their Environmental Entry and Predicted Fate, Springer, 3, 1-25, https://doi.org/10.1007/978-3-540-68331-5_1, 1997.

Alton, M. and Browne, E.: Atmospheric Chemistry of Volatile Methyl Siloxanes: Kinetics and Products of Oxidation by OH Radicals and Cl Atoms, Environ. Sci. Technol., 54, 5992-5999, https://dx.doi.org/10.1021/acs.est.0c01368, 2020.

Atkinson, R.: Kinetics of the Gas-Phase Reactions of a Series of Organosilicon Compounds with OH and NO_3 Radicals and O_3 at 297 ± 2 K, Environ. Sci. Technol., 25, 863-866, https://doi.org/10.1021/es00017a005, 1991.

Bein, K., Zhao, Y., Wexler, A., Johnston, M.: Speciation of Size-Resolved Individual Ultrafine Particles in

Pittsburgh, Pennsylvania, J. Geophys. Res., 110, D07S05, https://doi.org/10.1029/2004jd004708, 2005.

Berndt, T., Richters, S., Jokinen, T., Hyttinen, N., Kurtén, T., Otkjaer, R., Kjaergaard, H., Stratmann, F., Herrmann, H., Sipilä, M., Kulmala, M., and Ehn, M.: Hydroxyl Radical-Induced Formation of Highly Oxidized Organic Compounds, Nat. Commun., 7, 1-8, https://doi.org/10.1038/ncomms13677, 2016.

Bruns, E., Haddad, I., Keller, A., Klein, F., Kumar, N., Pieber, S., Corbin, J., Slowik, J., Brune, W., Baltensperger, U., and Prévôt, A.: Inter-Comparison of Laboratory Smog Chamber and Flow Reactor Systems on Organic Aerosol Yield and Composition, Atmos. Meas. Tech., 8, 2315-2332, https://doi.org/10.5194/amt-8-2315-2015, 2015.

Bzdek, B., Horan, A., Pennington, M., Janechek, N., Baek, J., Stanier, C., and Johnston, M.: Silicon is a Frequent Component of Atmospheric Nanoparticles, Environ. Sci. Technol., 48, 11137-11145, https://doi.org/10.1021/es5026933, 2014.

Canada, E. C. a. H.: https://www.ec.gc.ca/ese-ees/FC0D11E7-DB34-41AA-B1B3-E66EFD8813F1/batch2_540-97-6_en.pdf last access: 9 February 2022, 2008.

Chan, A., Kautzman, K., Chhabra, P., Surratt, J., Chan, M., Crounse, J., Kürten, A., Wennberg, P., Flagan, R., and Seinfeld, J.: Secondary Organic Aerosol Formation from Photooxidation of Naphthalene and Alkylnaphthalenes: Implications for Oxidation of Intermediate Volatility Organic Compounds (IVOCs), Atmos. Chem. Phys., 9, 3049–3060, https://doi.org/10.5194/acp-9-3049-2009, 2009.

Chandramouli, B., Kamens, R.: The Photochemical Formation and Gas-Particle Partitioning of Oxidation Products of Decamethyl Cyclopentasiloxane and Decamethyl Tetrasiloxane in the Atmosphere, Atmos. Environ., 35, 87-95, https://doi.org/10.1016/S1352-2310(00)00289-2, 2001.

Charan, S., Huang, Y., Buenconsejo, R., Li, Q., Cocker Iii, D., and Seinfeld, J.: Secondary Organic Aerosol Formation from the Oxidation of Decamethylcyclopentasiloxane at Atmospherically Relevant OH Concentrations, Atmos. Chem. Phys., 22, 917-928, https://doi.org/10.5194/acp-22-917-2022, 2022.

Coggon, M., McDonald, B., Vlasenko, A., Veres, P., Bernard, F., Koss, A., Yuan, B., Gilman, J., Peischl, J., Aikin, K., DuRant, J., Warneke, C., Li, S.-M., and Gouw, J.: Diurnal Variability and Emission Pattern of Decamethylcyclopentasiloxane (D5) from the Application of Personal Care Products in Two North American Cities, Environ. Sci. Technol., 52, 5610-5618, https://doi.org/10.1021/acs.est.8b00506, 2018.

EUR-Lex: https://eur-lex.europa.eu/legal-content/EN/TXT/?uri=uriserv:OJ.L_.2018.006.01.0045.01.ENG&toc=OJ:L:2018:006:TOCECHA, last access: 25 November 2021, 2018.

Farasani, A. and Darbre, P.: Exposure to Cyclic Volatile Methylsiloxanes (cVMS) Causes Anchorage-Independent Growth and Reduction of BRCA1 in Non-Transformed Human Breast Epithelial Cells, J. Appl. Toxicol., 37, 454-461, https://doi.org/10.1002/jat.3378, 2017.

Genualdi, S., Harner, T., Cheng, Y., Macleod, M., Hansen, K., Egmond, R., Shoeib, M., and Lee, S.: Global Distribution of Linear and Cyclic Volatile Methyl Siloxanes in Air, Environ. Sci. Technol., 45, 3349-3354, https://doi.org/10.1021/es200301j, 2011.

Glasius, M. and Goldstein, A.: Recent Discoveries and Future Challenges in Atmospheric Organic Chemistry, Environ. Sci. Technol., 50, 2754-2764, https://doi.org/10.1021/acs.est.5b05105, 2016.

Guo, J., Zhou, Y., Cui, J., Zhang, B., and Zhang, J.: Assessment of Volatile Methylsiloxanes in Environmental Matrices and Human Plasma, Sci. Total. Environ., 668, 1175-1182, https://doi.org/10.1016/j.scitotenv.2019.03.092, 2019.

Huang, Y., Coggon, M., Zhao, R., Lignell, H., Bauer, M., Flagan, R., and Seinfeld, J.: The Caltech Photooxidation Flow Tube reactor: Design, Fluid Dynamics and Characterization, Atmos. Meas. Tech., 10, 839-867, https://doi.org/10.5194/amt-10-839-2017, 2017.

Janechek, N., Hansen, K., and Stanier, C.: Comprehensive Atmospheric Modeling of Reactive Cyclic Siloxanes and their Oxidation Products, Atmos. Chem. Phys., 17, 8357-8370, https://doi.org/10.5194/acp-17-8357-2017, 2017.

Janechek, N., Marek, R., Bryngelson, N., Singh, A., Bullard, R., Brune, W., and Stanier, C.: Physical Properties of Secondary Photochemical Aerosol from OH Oxidation of a Cyclic Siloxane, Atmos. Chem. Phys., 19, 1649-1664, https://doi.org/10.5194/acp-19-1649-2019, 2019.

Jokinen, T., Berndt, T., Makkonen, R., Kerminen, V., Junninen, H., Paasonen, P., Stratmann, F., Herrmann, H., Guenther, A., Worsnop, D., Kulmala, M., Ehn, M., and Sipilä, M.: Production of Extremely Low Volatile Organic Compounds from Biogenic Emissions: Measured Yields and Atmospheric Implications, Proc. Natl. Acad. Sci. U S A., 112, 7123-7128, https://doi.org/10.1073/pnas.1423977112, 2015.

Kierkegaard, A. and McLachlan, M.: Determination of Linear and Cyclic Volatile Methylsiloxanes in Air at a Regional Background Site in Sweden, Atmos. Environ., 80, 322-329, https://doi.org/10.1016/j.atmosenv.2013.08.001, 2013.

Kim, J. and Xu, S.: Quantitative Structure-Reactivity Relationships of Hydroxyl Radical Rate Constants for Linear and Cyclic Volatile Methylsiloxanes, Environ. Toxicol. Chem., 36, 3240-3245, https://doi.org/10.1002/etc.3914, 2017.

Kim, J., Mackay, D., and Whelan, M.: Predicted Persistence and Response Times of Linear and Cyclic Volatile Methylsiloxanes in Global and Local Environments, Chemosphere, 195, 325-335, https://doi.org/10.1016/j.chemosphere.2017.12.071, 2018.

Krogseth, I., Zhang, X., Lei, Y., Wania, F., and Breivik, K.: Calibration and Application of a Passive Air Sampler (XAD-PAS) for Volatile Methyl Siloxanes, Environ. Sci. Technol., 47, 4463-4470, https://doi.org/10.1021/es400427h, 2013a.

Krogseth, I., Kierkegaard, A., McLachlan, M., Breivik, K., Hansen, K., and Schlabach, M.: Occurrence and Seasonality of Cyclic Volatile Methyl Siloxanes in Arctic Air, Environ. Sci. Technol., 47, 502-509, https://doi.org/10.1021/es3040208, 2013b.

Lambe, A., Chhabra, P., Onasch, T., Brune, W., Hunter, J., Kroll, J., Cummings, M., Brogan, J., Parmar, Y., Worsnop, D., Kolb, C., and Davidovits, P.: Effect of Oxidant Concentration, Exposure Time, and Seed Particles on Secondary Organic Aerosol Chemical Composition and Yield, Atmos. Chem. Phys., 15, 3063-3075, https://doi.org/10.5194/acp-15-3063-2015, 2015.

Lambe, A., Ahern, A., Williams, L., Slowik, J., Wong, J., Abbatt, J., Brune, W., Ng, N., Wright, J., Croasdale, D., Worsnop, D., Davidovits, P., and Onasch, T.: Characterization of Aerosol Photooxidation Flow Reactors: Heterogeneous Oxidation, Secondary Organic Aerosol Formation and Cloud Condensation Nuclei Activity Measurements, Atmos. Meas. Tech., 4, 445-461, https://doi.org/10.5194/amt-4-445-2011, 2011.

Lambe, A., Massoli, P., Zhang, X., Canagaratna, M., Nowak, J., Daube, C., Yan, C., Nie, W., Onasch, T., Jayne, J., Kolb, C., Davidovits, P., Worsnop, D., and Brune, W.: Controlled Nitric Oxide Production via $O(^1D) + N_2O$ Reactions for Use in Oxidation Flow Reactor Studies, Atmos. Meas. Tech., 10, 2283-2298, https://doi.org/10.5194/amt-10-2283-2017, 2017.

Lamkaddam, H., Gratien, A., Pangui, E., Cazaunau, M., Varrault, B., and Doussin, J.: High-NO_x Photooxidation of n-Dodecane: Temperature Dependence of SOA Formation, Environ Sci Technol, 51, 192-201, https://doi.org/10.1021/acs.est.6b03821, 2017.

Lee, A., Hayden, K., Herckes, P., Leaitch, W., Liggio, J., Macdonald, A., and Abbatt, J.: Characterization of Aerosol and Cloud Water at a Mountain Site During WACS 2010: Secondary Organic Aerosol Formation through Oxidative Cloud Processing, Atmos. Chem. Phys., 12, 7103-7116, https://doi.org/10.5194/acp-12-7103-2012, 2012.

Li, K., Liggio, J., Lee, P., Han, C., Liu, Q., and Li, S.-M.: Secondary Organic Aerosol Formation from α-Pinene, Alkanes, and Oil Sand-Related Precursors in a New Oxidation Flow Reactor, Atmos. Chem. Phys., 19, 9715-

9731, https://doi.org/10.5194/acp-19-9715-2019, 2019a.

Li, K., Liggio, J., Han, C., Liu, Q., Moussa, S., Lee, P., and Li, S.-M.: Understanding the Impact of High-NO_x Conditions on the Formation of Secondary Organic Aerosol in the Photooxidation of Oil Sand-Related Precursors, Environ. Sci. Technol., 53, 14420-14429, https://doi.org/10.1021/acs.est.9b05404, 2019b.

Li, Q., Lan, Y., Liu, Z., Wang, X., Wang, X., Hu, J., and Geng, H.: Cyclic Volatile Methylsiloxanes (cVMSs) in the Air of the Wastewater Treatment Plants in Dalian, China-Levels, Emissions, and Trends, Chemosphere, 256, 1-8, https://doi.org/10.1016/j.chemosphere.2020.127064, 2020.

Li, S.-M. and Winchester, J.: Particle Size Distribution and Chemistry of Late Winter Arctic Aerosols, J. Geophys. Res., 95, 13897-13908, https://doi.org/10.1029/J095iD09p13897, 1990.

Li, S.-M. and Winchester, J.: Aerosol Silicon and Associated Elements in the Arctic High and Mid-Troposphere, Atmos. Environ., 27, 2907-2912, https://doi.org/10.1016/0960-1686(93)90322-P, 1993.

Liggio, J., Li, S.-M., Hayden, K., Taha, Y., Stroud, C., Darlington, A., Drollette, B., Gordon, M., Lee, P., Liu, P., Leithead, A., Moussa, S., Wang, D., Brien, J., Mittermeier, R., Brook, J., Lu, G., Staebler, R., Han, Y., Tokarek, T., Osthoff, H., Makar, P., Zhang, J., Plata, D., and Gentner, D.: Oil Sands Operations as a Large Source of Secondary Organic Aerosols, Nature, 534, 91-94, https://doi.org/10.1038/nature17646, 2016.

Liu, N., Xu, L., and Cai, Y.: Methyl Siloxanes in Barbershops and Residence Indoor Dust and the Implication for Human Exposures, Sci. Total. Environ., 618, 1324-1330, https://doi.org/10.1016/j.scitotenv.2017.09.250, 2018.

Mao, J., Ren, X., Brune, W., Olson, J., Crawford, J., Fried, A., Huey, L., Cohen, R., Heikes, B., Singh, H., Blake, D., Sachse, G., Diskin, G., Hall, S., and Shetter, R.: Airborne Measurement of OH Reactivity during INTEX-B, Atmos. Chem. Phys., 9, 163-173, https://doi.org/10.5194/acp-9-163-2009, 2009.

McFiggans, G., Mentel, T., Wildt, J., Pullinen, I., Kang, S., Kleist, E., Schmitt, S., Springer, M., Tillmann, R., Wu, C., Zhao, D., Hallquist, M., Faxon, C., Breton, M., Hallquist, A., Simpson, D., Bergström, R., Jenkin, M., Ehn, M., Thornton, J., Alfarra, M., Bannan, T., Percival, C., Priestley, M., Topping, D., and Scharr, A.: Secondary Organic Aerosol Reduced by Mixture of Atmospheric Vapours, Nature, 565, 587-593, https://doi.org/10.1038/s41586-018-0871-y, 2019.

Milani, A., Al-Naiema, I., and Stone, E.: Detection of a Secondary Organic Aerosol Tracer Derived from Personal Care Products, Atmos. Environ., 246, https://doi.org/10.1016/j.atmosenv.2020.118078, 2021.

Ng, N., Kroll, J., Chan, A., Chhabra, P., Flagan, R., and Seinfeld, J.: Secondary Organic Aerosol Formation from m-Xylene, Toluene, and Benzene, Atmos. Chem. Phys., 7, 3909–3922, https://doi.org/10.5194/acp-7-3909-2007, 2007a.

Ng, N., Chhabra, P., Chan, A., Surratt, J., Kroll, J., Kwan, A., McCabe, D., Wennberg, P., Sorooshian, A., Murphy, S., Dalleska, N., Flagan, R., and Seinfeld, J.: Effect of NO_x Level on Secondary Organic Aerosol (SOA) Formation from the Photooxidation of Terpenes, Atmos. Chem. Phys., 7, 5159–5174, https://doi.org/10.5194/acp-7-5159-2007, 2007b.

Ng, N., Canagaratna, M., Zhang, Q., Jimenez, J., Tian, J., Ulbrich, I., Kroll, J., Docherty, K., Chhabra, P., Bahreini, R., Murphy, S., Seinfeld, J., Hildebrandt, L., Donahue, N., DeCarlo, P., Lanz, V., Prévôt, A., Dinar, E., Rudich, Y., and Worsnop, D.: Organic Aerosol Components Observed in Northern Hemispheric Datasets from Aerosol Mass Spectrometry, Atmos. Chem. Phys., 10, 4625-4641, https://doi.org/10.5194/acp-10-4625-2010, 2010.

Peng, Z., Taylor, J., Orlando, J., Tyndall, G., and Jimenez, J.: Organic Peroxy Radical Chemistry in Oxidation Flow Reactors and Environmental Chambers and their Atmospheric Relevance, Atmos. Chem. Phys., 19, 813-834, https://doi.org/10.5194/acp-19-813-2019, 2019.

Peng, Z., Palm, B., Day, D., Talukdar, R., Hu, W., Lambe, A., Brune, W., and Jimenez, J.: Model Evaluation of New Techniques for Maintaining High-NO Conditions in Oxidation Flow Reactors for the Study of OH-Initiated Atmospheric Chemistry, ACS. Earth. Space. Chem. , 2, 72-86, https://doi.org/10.1021/acsearthspacechem.7b00070, 2018.

Pennington, E., Seltzer, K., Murphy, B., Qin, M., Seinfeld, J., and Pye, H.: Modeling Secondary Organic Aerosol Formation from Volatile Chemical Products, Atmos. Chem. Phys., 21, 18247-18261, https://doi.org/10.5194/acp-21-18247-2021, 2021.

Phares, D., Rhoads, K., Johnston, M., and Wexler, A.: Size-Resolved Ultrafine Particle Composition Analysis 2. Houston, J. Geophys. Res., 108, 1-14, https://doi.org/10.1029/2001jd001212, 2003.

Presto, A., Hartz, K., and Donahue, N.: Secondary Organic Aerosol Production from Terpene Ozonolysis. 2. Effect of NO_x Concentration, Environ. Sci. Technol. , 39, 7046-7054, https://doi.org/10.1021/es050400s, 2005.

Rauert, C., Shoieb, M., Schuster, J., Eng, A., and Harner, T.: Atmospheric Concentrations and Trends of Poly- and Perfluoroalkyl Substances (PFAS) and Volatile Methyl Siloxanes (VMS) over 7 Years of Sampling in the Global Atmospheric Passive Sampling (GAPS) Network, Environ. Pollut., 238, 94-102, https://doi.org/10.1016/j.envpol.2018.03.017, 2018.

Rhoads, K., Phares, D., Wexler, A., Johnston, M.: Size-Resolved Ultrafine Particle Composition Analysis 1. Atlanta, J. Geophys. Res., 108, 1-13, https://doi.org/10.1029/2001jd001211, 2003.

Riipinen, I., Juuti, T., Pierce, J., Petäjä, T., Worsnop, D., Kulmala, M., and Donahue, N.: The Contribution of Organics to Atmospheric Nanoparticle Growth, Nat. Geosci., 5, 453-458, https://doi.org/10.1038/ngeo1499,

2012.

Rücker, C. and Kümmerer, K.: Environmental Chemistry of Organosiloxanes, Chem. Rev., 115, 466-524, https://doi.org/10.1021/cr500319v, 2015.

Safron, A., Strandell, M., Kierkegaard, A., and Macleod, M.: Rate Constants and Activation Energies for Gas-Phase Reactions of Three Cyclic Volatile Methyl Siloxanes with the Hydroxyl Radical, Int. J. Chem. Kinet., 47, 420-428, https://doi.org/10.1002/kin.20919, 2015.

Sakurai, T., Imaizumi, Y., Kuroda, K., Hayashi, T., and Suzuki, N.: Georeferenced multimedia environmental fate of volatile methylsiloxanes modeled in the populous Tokyo Bay catchment basin, Sci Total Environ, 689, 843-853, https://doi.org/10.1016/j.scitotenv.2019.06.462, 2019.

Sarrafzadeh, M., Wildt, J., Pullinen, I., Springer, M., Kleist, E., Tillmann, R., Schmitt, S., Wu, C., Mentel, T., Zhao, D., Hastie, D., and Scharr, A.: Impact of NO_x and OH on Secondary Organic Aerosol Formation from β-Pinene Photooxidation, Atmos. Chem. Phys., 16, 11237-11248, https://doi.org/10.5194/acp-16-11237-2016, 2016.

Simonen, P., Saukko, E., Karjalainen, P., Timonen, H., Bloss, M., Saksa, P., Rönkkö, T., Keskinen, J., and Maso, M.: A New Oxidation Flow Reactor for Measuring Secondary Aerosol Formation of Rapidly Changing Emission Sources, Atmos. Meas. Tech., 10, 1519-1537, https://doi.org/10.5194/amt-10-1519-2017, 2017.

Sommerlade, R., Parlar, H., Wrobel, D , Kochs, P.: Product Analysis and Kinetics of the Gas-Phase Reactions of Selected Organosilicon Compounds with OH Radicals Using a Smog Chamber-Mass Spectrometer System, Environ. Sci. Technol., 27, 2435-2440, https://doi.org/10.1021/es00048a019, 1993.

Tang, X., Misztal, P., Nazaroff, W., and Goldstein, A.: Siloxanes Are the Most Abundant Volatile Organic Compound Emitted from Engineering Students in a Classroom, Environ. Sci. Technol. Lett. , 2, 303-307, https://doi.org/10.1021/acs.estlett.5b00256, 2015.

Tkacik, D., Lambe, A., Jathar, S., Li, X., Presto, A., Zhao, Y., Blake, D., Meinardi, S., Jayne, J., Croteau, P., and Robinson, A.: Secondary Organic Aerosol Formation from in-Use Motor Vehicle Emissions Using a Potential Aerosol Mass Reactor, Environ. Sci. Technol., 48, 11235-11242, https://doi.org/10.1021/es502239v, 2014.

Wang, D.-G., Norwood, W., Alaee, M., Byer, J., and Brimble, S.: Review of Recent Advances in Research on the Toxicity, Detection, Occurrence and Fate of Cyclic Volatile Methyl Siloxanes in the Environment, Chemosphere, 93, 711-725, https://doi.org/10.1016/j.chemosphere.2012.10.041, 2013.

Wang, X., Schuster, J., Jones, K., and Gong, P.: Occurrence and Spatial Distribution of Neutral Perfluoroalkyl Substances and Cyclic Volatile Methylsiloxanes in the Atmosphere of the Tibetan Plateau, Atmos. Chem. Phys., 18, 8745-8755, https://doi.org/10.5194/acp-18-8745-2018, 2018.

651 Wang, X., Lee, S., Sheng, G., Chan, L., Fu, J., Li, X., Min, Y., and Chan, C.: Cyclic organosilicon compounds in
652 ambient air in Guangzhou, Macau and Nanhai, Pearl River Delta, Appl. Geochemistry, 16, 1447-1454,
653 https://doi.org/10.1016/S0883-2927(01)00044-0, 2001.
654 Wildt, J., Mentel, T., Scharr, A., Hoffmann, T., Andres, S., Ehn, M., Kleist, E., Müsgen, P., Rohrer, F., Rudich, Y.,
655 Springer, M., Tillmann, R., and Wahner, A.: Suppression of New Particle Formation from Monoterpene
656 Oxidation by NO_x, Atmos. Chem. Phys., 14, 2789-2804, https://doi.org/10.5194/acp-14-2789-2014, 2014.
657 Wu, Y. and Johnston, M.: Molecular Characterization of Secondary Aerosol from Oxidation of Cyclic
658 Methylsiloxanes, J. Am. Soc. Mass Spectrom., 27, 402-409, https://doi.org/10.1007/s13361-015-1300-1, 2016.
659 Wu, Y. and Johnston, M.: Aerosol Formation from OH Oxidation of the Volatile Cyclic Methyl Siloxane (cVMS)
660 Decamethylcyclopentasiloxane, Environ. Sci. Technol., 51, 4445-4451,
661 https://doi.org/10.1021/acs.est.7b00655, 2017.
662 Xiao, R., Zammit, I., Wei, Z., Hu, W.-P., MacLeod, M., and Spinney, R.: Kinetics and Mechanism of the Oxidation
663 of Cyclic Methylsiloxanes by Hydroxyl Radical in the Gas Phase: An Experimental and Theoretical Study,
664 Environ. Sci. Technol., 49, 13322-13330, https://doi.org/10.1021/acs.est.5b03744, 2015.
665 Xu, S., Warner, N., Nizzetto, P., Durham, J., and McNett, D.: Long-Range Transport Potential and Atmospheric
666 Persistence of Cyclic Volatile Methylsiloxanes Based on Global Measurements, Chemosphere, 228, 460-468,
667 https://doi.org/10.1016/j.chemosphere.2019.04.130, 2019.
668 Zhao, D., Schmitt, S., Wang, M., Acir, I., Tillmann, R., Tan, Z., Novelli, A., Fuchs, H., Pullinen, I., Wegener, R.,
669 Rohrer, F., Wildt, J., Scharr, A., Wahner, A., and Mentel, T.: Effects of NO_x and SO_2 on the Secondary Organic
670 Aerosol Formation from Photooxidation of α-Pinene and Limonene, Atmos. Chem. Phys., 18, 1611-1628,
671 https://doi.org/10.5194/acp-18-1611-2018, 2018.
672 Zhou, C., Jang, M., and Yu, Z.: Simulation of SOA Formation from the Photooxidation of Monoalkylbenzenes in
673 the Presence of Aqueous Aerosols Containing Electrolytes under Various NO_x Levels, Atmos. Chem. Phys., 19,
674 5719-5735, https://doi.org/10.5194/acp-19-5719-2019, 2019.